IEEE Photonics Journal
An IEEE Photonics Society Publication

Open Access

Titanium Dioxide Hole-Blocking Layer in Ultra-Thin-Film Crystalline Silicon Solar Cells

Volume 11, Number 6, December 2019

Yangsen Kang
Huiyang Deng
Yusi Chen
Yijie Huo
Jieyang Jia
Li Zhao
Zain Zaidi
Kai Zang
James S. Harris

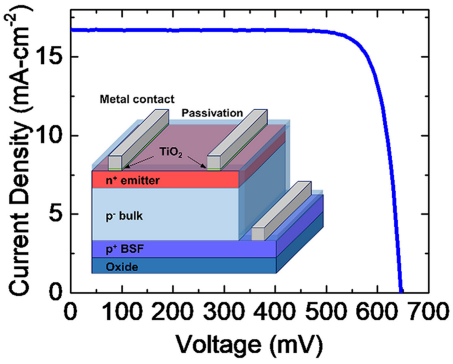

DOI: 10.1109/JPHOT.2019.2947582

IEEE photonics SOCIETY

IEEE

Titanium Dioxide Hole-Blocking Layer in Ultra-Thin-Film Crystalline Silicon Solar Cells

Yangsen Kang, Huiyang Deng, Yusi Chen, Yijie Huo, Jieyang Jia, Li Zhao, Zain Zaidi, Kai Zang, and James S. Harris

Department of Electrical Engineering, Stanford University, CA 94305 USA

DOI:10.1109/JPHOT.2019.2947582

Manuscript received September 16, 2019; revised October 5, 2019; accepted October 10, 2019. Date of publication October 15, 2019; date of current version October 24, 2019. This work was supported in part by the Bay Area Photovoltaic Consortium and in part by the Global Climate and Energy Project at Stanford University. *Yangsen Kang and Huiyang Deng contributed equally to this work*. Corresponding author: Huiyang Deng (e-mail: huiyang_deng@alumni.stanford.edu).

Abstract: One of the remaining obstacles to achieving the theoretical efficiency limit of crystalline silicon (c-Si) solar cells is high interface recombination loss for minority carriers at the Ohmic contacts. The contact recombination loss of the ultra-thin-film c-Si solar cells is more severe than that of the state-of-art thick cells due to the smaller volume and higher minority carrier concentration. This paper presents a design of an electron passing (Ohmic) contact for n-type Si that is hole-blocking with significantly reduced hole recombination. By depositing a thin titanium dioxide (TiO_2) layer, we form a metal-insulator-semiconductor (MIS) contact for a 2 μm-thick Si cell to achieve an open circuit voltage (V_{oc}) of 645 mV, which is 10 mV higher than that of an ultra-thin cell with a traditional metal contact. This TiO_2 MIS contact constitutes a step towards high-efficiency ultra-thin-film c-Si solar cells.

Index Terms: Silicon photovoltaic, ultra-thin-film, selective contact, titanium dioxide.

1. Introduction

Ultra-Thin-Film crystalline silicon (c-Si) solar cells have attracted great interest due to their potential of lowering the cost and increasing the efficiency of c-Si solar cells [1]–[4]. As the recombination loss in the bulk Si is substantially reduced because of the thickness reduction of solar cells, the recombination loss at surfaces, especially the metal Ohmic contacts, becomes the main obstacle for high performance. The key to solve this issue is forming carrier-selective contacts in c-Si solar cells, which can provide lower minority carrier recombination velocity as well as more efficient majority carrier transport.

Traditional c-Si solar cells use a diffused emitter and back surface field (BSF) to create carrier-selective layers. It has been shown that recombination at the metal/silicon interface still causes more than 40% of the total recombination losses [5], [6]. To further control the contact recombination loss, various advanced cell designs have been demonstrated. One example is the heterojunction solar cell with an intrinsic larger bandgap thin-film (HIT) [7]–[9]. Nevertheless, the a-Si:H layer in HIT cells has high parasitic absorption and defect concentrations that result in a loss in the short circuit current (J_{sc}) [10], [11]. Another method is to deposit a thin tunneling silicon dioxide (SiO_2) layer as a carrier selective contact [12]–[14], [27]. To achieve low contact resistance, the thickness of the tunneling SiO_2 layer has to be precisely controlled, which could be challenging for large-scale manufacturing.

Recently, c-Si solar cells with Si/metal-oxide heterojunctions have been demonstrated, providing an alternative solution of carrier-selective layer [15]–[18]. However, those designs suffer the quality of surface passivation and the low V_{oc}.

TiO_2 has been widely used for perovskite and organic solar cells as selective contacts [23]–[26]. In this paper, we report a TiO_2-based carrier-selective contact for ultra-thin-film c-Si solar cell to effectively block holes without compromising the conductivity for electrons. By depositing a thin layer of TiO_2 between the metal and n-type Si, we form a metal-insulator-semiconductor (MIS) contact. TiO_2 has a large valance band (VB) offset (ΔE_v), causing holes to be blocked. Meanwhile, passivation can be provided by TiO_2 on an n-type Si surface, achieving a surface recombination velocity (SRV) as low as 100 cm-sec^{-1} [18]–[20]. Thereby, TiO_2 can prevent holes from recombining at this interface or diffusing into the metal. For the conduction band (CB), TiO_2 can unpin the Fermi level at the Si surface, eliminate the Schottky barrier, and pin the Fermi level of the metal close to the CB edge of Si [20], [21]. This MIS contact has a small CB offset (ΔE_c), allowing electrons to transport freely through the hole blocking layer. With the aligned CB, this MIS contact also exhibits high tolerance for variations in the thickness of the TiO_2 layer. We experimentally demonstrate a TiO_2 carrier-selective contact on an ultra-thin-film c-Si junction solar cell, which can reduce the SRV at the contacts and suppress the recombination current. In experiment, a 2 μm-thick c-Si solar cell with the TiO_2 MIS hole-blocking contact has achieved a V_{oc} of 645 mV, which is 10 mV higher than the control group (a 2 μm-thick c-Si solar cell with a traditional metal contact).

2. Design and Simulation

To show the advantages of carrier-selective contacts in c-Si solar cells, we simulated the effects of applying carrier-selective contacts to various Si solar cells using Synopsys Technology Computer-Aided Design (TCAD). These simulations consider both intrinsic recombination (Auger and radiative recombination) and extrinsic recombination (Shockley-Read-Hall (SRH), surface and contact recombination). The simulated cell structure is illustrated in Fig. 1(a), which consists of a lightly p-doped bulk absorber (doping concentration 10^{16} cm^{-3}), 50 nm of n^+ emitter (doping concentration 10^{20} cm^{-3}), and 50 nm of p^+ back surface field (BSF) layer (doping concentration 10^{20} cm^{-3}). The cell thickness varies from 1 μm to 100 μm and the minority carrier lifetime is assumed to be 1 ms. In order to demonstrate the effects of carrier-selective contacts, the minority carrier recombination velocity at the contacts is set at 10^2 cm-sec^{-1} for both electron and hole selective contacts and 10^7 cm-sec^{-1} for metal contacts. The surface recombination velocity (SRV) at the passivated surfaces is assumed to be 10 cm-sec^{-1}. The recombination currents are analyzed under different mechanisms, including bulk, BSF, emitter, and contact recombination. The bulk recombination current accounts for the SRH, Auger and radiative recombination in the bulk region. The front/rear recombination current includes all the recombination at the emitter/BSF and at the front/rear interfaces. The contact recombination current includes the recombination at both front and rear contacts.

The V_{oc} of cells with and without carrier-selective contacts are plotted versus the cell thickness in Fig. 1(b). It can be observed from this plot that the carrier-selective contact can improve the V_{oc} of cells with thickness from 1 μm to 100 μm, with the enhancement far more prominent in the thinner cells. In the 1 μm cell, the carrier-selective contact improves the V_{oc} by 60 mV, while the carrier-selective contact improves the V_{oc} by 12 mV in the 100 μm thick cell. Such a difference in V_{oc} enhancement for different cell thicknesses can be explained by analyzing the components of the recombination current density J_0, as shown in Fig. 1(c). In a 1 μm thick cell with metal contacts, the contact recombination current ($J_{0,contact}$) is significantly larger than the other components, contributing to $\sim$90% of J_0. Applying carrier-selective contacts effectively suppresses this $J_{0,contact}$ and reduces J_0 from 12 fA-cm^{-2} to 1.2 fA-cm^{-2}, resulting in a V_{oc} improvement of 60 mV in the 1 μm thick cell. In the 100 μm thick cell with metal contacts, bulk and contact recombination current each contribute to $\sim$40% of the total recombination current. Carrier-selective contacts can therefore only reduce J_0 from 24 fA-cm^{-2} to 15 fA-cm^{-2} and improve V_{oc} by 12 mV, which is less significant than in the thin cells.

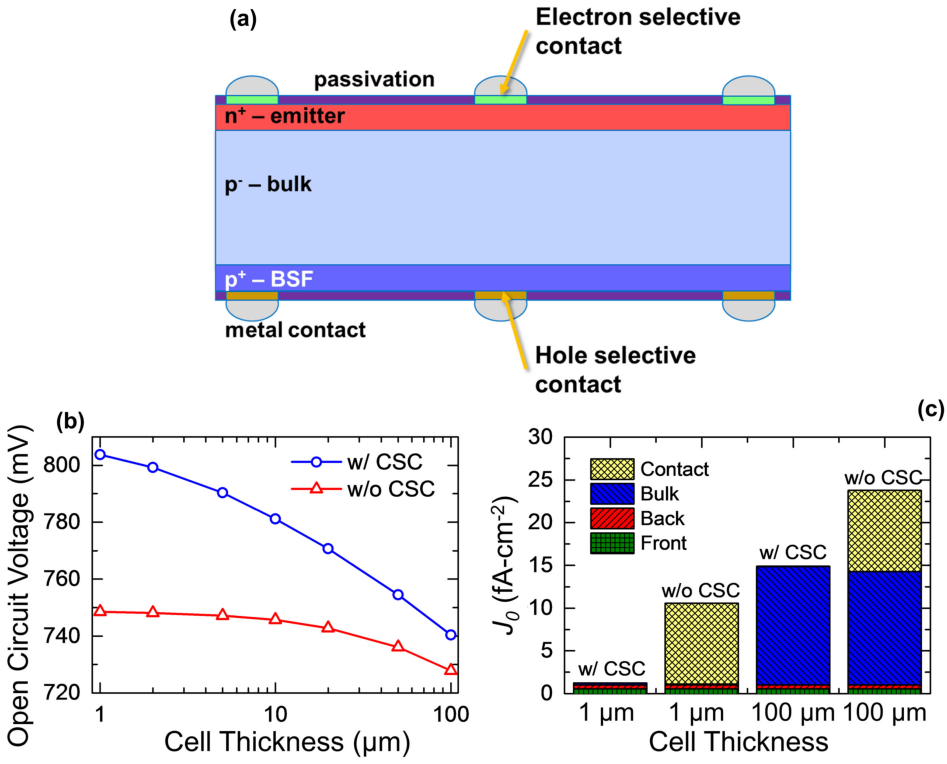

Fig. 1. (a) Schematic illustration of the simulated c-Si solar cell with carrier selective contacts. (b) Simulation results of V_{oc} as functions of the cell thickness with (blue circle) and without (red triangle) carrier-selective contacts (CSC). (c) Recombination current density (J_0) breakdown for 1 μm and 100 μm thick Si solar cells with and without CSC.

On the other hand, applying carrier-selective contacts enhances the increase in V_{oc} achieved through decreasing the cell thickness. In the metal contact cell, the V_{oc} is increased by only 20 mV as the cell thickness decreases from 100 μm to 1 μm, while that change is enhanced to 60 mV in the carrier-selective contact cells. Especially, the $J_{0,\,contact}$ in the metal contact cells becomes the majority term in J_0 when the cell is thinned down below 10 μm. Since such recombination does not scale with the change of thicknesses, the increase of V_{oc} becomes saturated in the metal contact thin cells. Applying carrier-selective contacts can significantly reduce $J_{0,contact}$, leading to a regime where the bulk recombination becomes the dominant recombination mechanism. The benefit of V_{oc} from the decrease in cell thickness remains in all cases, even in extremely thin cells. Therefore, carrier-selective contacts are important for achieving high voltage and high efficiency in thin c-Si cells with thickness below 10 μm.

3. Device Fabrication and Characterization

Our ultra-thin-film c-Si solar cells (illustrated in Fig. 2(a)) are fabricated on a silicon-on-insulator (SOI) wafer to precisely control the cell thickness. Each cell is 2 $\times$ 2 mm in dimension. The active area of each device is 0.0221 cm^2 excluding the shaded area due to the metal contacts. The buried oxide blocks carriers generated in the thick Si substrate. The active region of the cells is epitaxially deposited by chemical vapor deposition (CVD). First, a layer of 100 nm thick 10^{19} cm^{-3} boron doped p$^+$ Si and a layer of 400 nm thick 10^{17} cm^{-3} boron doped Si are grown to form the BSF. Then 1000 nm thick lightly ($\sim 10^{16}$ cm^{-3}) boron doped base is grown. Last, a 400 nm thick 10^{18} cm^{-3} phosphorus doped n$^+$ Si region and a 100 nm thick 10^{19} cm^{-3} phosphorus doped n$^+$ Si region are grown to form the emitter. After this junction formation, trench isolation and mesa definition were done by photolithography and dry etch. The wafer is then oxidized in water vapor at

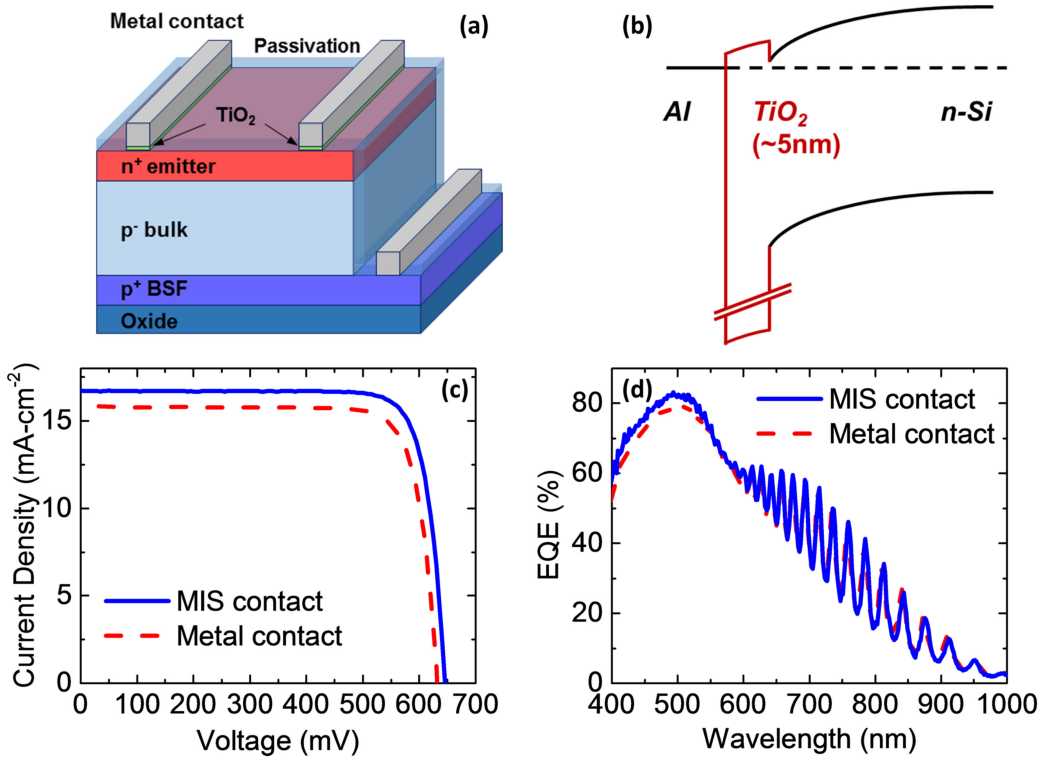

Fig. 2. (a) Schematic of the ultra-thin-film c-Si solar cell with the TiO_2 MIS contact. (b) Band diagram of the TiO_2 MIS contact. (c) Current-density-voltage characteristics of the ultra-thin-film c-Si solar cells with TiO_2 MIS contacts (blue solid line) and with metal contacts (red dash line). (d) External quantum efficiency (EQE) of 2 μm-thick Si solar cells with TiO_2 MIS contacts (blue solid line) and with metal contacts (red dash line).

950 °C to grow 100 nm thick thermal oxide to passivate the Si surface. The top contact pattern is then defined by lithography, and thermal oxide is wet etched to open the contact area. 5 nm thick TiO_2 is deposited by atomic layer deposition (ALD) using a precursor of Tetrakis (dimethylamido) titanium (IV) and DI water steam at 200 °C in 132 cycles. The thickness of 5 nm is chosen for effective hole blocking [21]. The pulse duration for Tetrakis (dimethylamido) titanium (IV) and DI water steam are 0.3 s and 0.015 s respectively. The purge time is 20 s between two pulses. The N_2 flow rate is 5 sccm. A metal contact of 10 nm thick titanium (Ti) and 200 nm thick aluminum (Al) is e-beam evaporated immediately after the deposition of TiO_2 to prevent degradation of the TiO_2 ALD film. After metallization, reactive-ion etching (RIE) is performed to etch away all the remaining TiO_2 on the wafer to prevent shunting. The bottom contacts are defined by lithography and formed by the evaporation of Ti (20 nm) and Al (300 nm). To optimize toward the best performance, cells are annealed under forming gas at different temperatures in the range from 300 °C to 500 °C for 90 seconds. Finally, the thermal oxide is thinned down to ~80 nm by dry etching to function as the single layer anti-reflective coating. Control samples without the TiO_2 layer are fabricated with an identical process except that the TiO_2 deposition step is skipped.

Solar cell efficiency is measured under air mass (AM) 1.5G normal illumination (1000 W/m^2, 1 sun) at room temperature. A standard solar simulator is used as the light source, with its intensity monitored by a certified photodetector. For the external quantum efficiency (EQE) measurement, a mechanically chopped monochromatic light beam is used as the light source, and the photocurrent is measured using a lock-in amplifier. The light intensity for the EQE measurement is calibrated with an amplified, calibrated photodetector. The saturation current is measured using the quasi-steady-state open circuit voltage (QSSV_{oc}) method with a Sinton Instrument WCT-120.

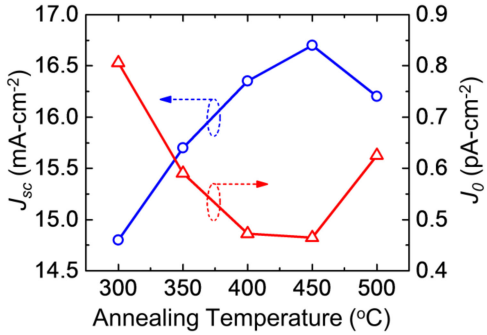

Fig. 3. Measured J_{sc} (blue circle) and J_0 (red triangle) as a function of annealing temperature.

4. Results and Discussion

Fig. 2(c) shows the current-density-voltage (*J-V*) characteristics of the devices measured under AM 1.5 solar spectrum. The 2 μm thick c-Si cell with a TiO_2 MIS contact achieves a V_{oc} of 645 mV, a J_{sc} of 16.7 mA-cm^{-2}, and an efficiency η of 8.9%. Compared to the cell with metal contacts, the cell with MIS contacts demonstrates an enhancement in both V_{oc} and J_{sc}. The V_{oc} of 645 mV in the MIS contact cell is 10 mV higher than that of the metal contact cell, which is mainly due to the reduced contact recombination loss. The quasi-steady-state V_{oc} (QSSV_{oc}) characterization shows a recombination current density (J_0) of 0.46 pA-cm^{-2} in the MIS contact cell and a J_0 of 0.72 pA-cm^{-2} in the metal contact cell. This 40% drop of J_0 reflects a significant reduction in the recombination velocity at the contact interface under the TiO_2 MIS contacts. For a cell with a thickness of 2 μm, our simulation suggests that the $J_{0,contact}$ contributes to 80%–90% of J_0. The electron-selective contact can suppress the recombination at the top contact and thus reduce the $J_{0,contact}$ by half, resulting in a ~40% reduction of J_0 and consequently the 10 mV V_{oc} enhancement in our cell with TiO_2 MIS contacts.

The MIS contact cell shows a 0.9 mA-cm^{-2} higher J_{sc} than the metal contact cell, which is mainly a result of the improved carrier collection efficiency due to the suppressed minority carrier recombination at the TiO_2 MIS contact. Under the light condition, the shadowing from metal fingers causes the minority carrier concentration under the contact being much lower than that in the illuminated area. The light generated carriers can diffuse toward the contact and cause a significant recombination loss. This loss could affect the minority carriers up to a few diffusion lengths away from the contact in the lateral direction. Thus, reducing contact recombination loss could benefit both J_{sc} and V_{oc}. Fig. 2(d) shows the measured external quantum efficiency (EQE) of cells with TiO_2 MIS contacts versus with metal contacts. It can be seen that the photon response of the MIS contact cell is clearly improved in the wavelength range of 400 nm–550 nm, since photons in this wavelength range are absorbed near the top surface within the emitter in our device. The TiO_2 MIS contact can suppress recombination by pushing more carriers toward the depletion region, and thus boost the carrier collection efficiency. In the long wavelength range, the EQE of the 2 μm thick cell is considerably decreased due to the insufficient absorption of Si. As suggested in previous research, this issue can be resolved by applying nano-scale light trapping structures. Besides, if we include light trapping in the near future, the efficiency of this solar cell could be significantly improved due to increased J_{sc} [1]–[3].

The key to the TiO_2 MIS contact is the property of interface passivation at the TiO_2/n-Si interface, which can be improved by post deposition annealing [20]. Samples with TiO_2 MIS contacts were annealed in forming gas at different temperatures ranging from 300 °C to 500 °C for 90 seconds. In Fig. 3, it can be seen that as the annealing temperature increases from 300 °C to 450 °C, J_{sc} increases significantly by 13% and J_0 drops by 43%, which is equivalent to 16 mV increases in V_{oc}. These results show that annealing improves the passivation effect of TiO_2 as well as the EQE at short wavelengths. As the annealing temperature further increases to 500 °C, J_0 increases by 38%

TABLE 1
Key Performance Parameters of 2 μm Thick Si Solar Cells

	V_{oc} (mV)	J_{sc} (mA-cm^{-2})	F.F. (%)	η (%)	J_0 (pA-cm^{-2})
TiO_2 MIS Contact	645	16.7	82.2	8.9	0.46
Metal Contact	635	15.8	81.6	8.2	0.72

and J_{sc} drops by 3% compared to the optimized condition. These are probably due to degradation of the passivation effect, which could be caused by a phase change of TiO_2 from anatase to rutile at high temperature [21], [22]. Annealing at 450 °C produces the best device with the lowest J_0 of 4.6 pA-cm^{-2}, highest J_{sc} of 16.7 mA-cm^{-2} and best efficiency of 8.9%. The performance of this device and its control group is detailed in Table 1.

5. Conclusions

In summary, we have demonstrated a carrier-selective contact with a TiO_2 MIS structure. With this carrier-selective contact, a 2 μm-thick Si solar cell has achieved a V_{oc} of 645 mV, which is 10 mV higher than that of a comparable cell with metal contact. We use TCAD simulations to analyze the recombination loss in thin cells and to reveal why the V_{oc} is improved by the MIS contact. Our results show that eliminating contact recombination, a major recombination mechanism in thin cells, is essential to the design of high-efficiency c-Si cells. We have also performed post deposition annealing of TiO_2 MIS contact cells to further enhance the effect brought by this carrier-selective contact. Overall, we report a design of TiO_2 carrier-selective contacts and demonstrate its application in ultra-thin-film c-Si solar cells.

Acknowledgment

The authors acknowledge Stanford Nanofabrication Facility (SNF) for the use of the processing facilities, and would like to thank P. Beck for experimental support, and J. Renshaw and S. Chatterjee for characterization support.

References

[1] S. Jeong, M. D. McGehee, and Y. Cui, "All-back-contact ultra-thin silicon nanocone solar cells with 13.7% power conversion efficiency," *Nature Commun.*, vol. 4, 2013, Art. no. 2950.
[2] R. A. Pala, J. White, E. Barnard, J. Liu, and M. L. Brongersma, "Design of plasmonic thin-film solar cells with broadband absorption enhancements," *Adv. Mater.*, vol. 21, no. 34, pp. 3504–3509, 2009.
[3] M. S. Branham *et al.*, "15.7% efficient 10-μm-thick crystalline silicon solar cells using periodic nanostructures," *Adv. Mater.*, vol. 27, no. 13, pp. 2182–2188, 2015.
[4] W. Lu *et al.*, "Development of a 16.8% efficient 18-μm silicon solar cell on steel," *IEEE J. Photovolt.*, vol. 4, no. 6, pp. 1397–1404, Nov. 2014.
[5] SEMI PV Group, Int. Technol. Roadmap. Photovolt., Frankfurt, Germany, 2013.
[6] L. Tous *et al.*, "Evaluation of advanced p-PERL and n-PERT large area silicon solar cells with 20.5% energy conversion efficiencies," *Prog. Photovolt.: Res. Appl.*, vol. 23, no. 5, pp. 660–670, 2015.
[7] M. Lu, S. Bowden, U. Das, and R. Birkmire, "Interdigitated back contact silicon heterojunction solar cell and the effect of front surface passivation," *Appl. Phys. Lett.*, vol. 91, no. 6, 2007, Art. no. 063507.
[8] K. Masuko *et al.*, "Interdigitated back contact silicon heterojunction solar cell and the effect of front surface passivation," *Appl. Phys. Lett.*, vol. 91, no. 6, 2007, Art. no. 063507.
[9] D. Pysch *et al.*, "Comparison of intrinsic amorphous silicon buffer layers for silicon heterojunction solar cells deposited with different PECVD Techniques," in *Proc. 35th IEEE Photovol. Specialists Conf.*, Jun. 2010, pp. 3570–3576.
[10] S. De Wolf, A. Descoeudres, C. H. Zachary, and C. Ballif, "High-efficiency silicon heterojunction solar cells: A review," *Green*, vol. 2, no. 1, pp. 7–24, 2012.

[11] Z. C. Holman *et al.*, "Current losses at the front of silicon heterojunction solar cells," *IEEE J. Photovolt.*, vol. 2, no. 1, pp. 7–15, Jan. 2012.
[12] F. Feldmann, M. Simon, M. Bivour, C. Reichel, M. Hermle, and S. W. Glunz, "Carrier-selective contacts for Si solar cells," *Appl. Phys. Lett.*, vol. 104, no. 18, 2014, Art. no. 181105.
[13] J. B. Heng *et al.*, "$>$23% high-efficiency tunnel oxide junction bifacial solar cell with electroplated Cu gridlines," *IEEE J. Photovolt.*, vol. 5, no. 1, pp. 82–86, Jan. 2014.
[14] D. L. Young, W. Nemeth, S. Grover, A. Norman, B. G. Lee, and P. Stradins, "Carrier-selective, passivated contacts for high efficiency silicon solar cells based on transparent conducting oxides," in *Proc. IEEE 40th Photovolt. Specialist Conf.*, 2014, pp. 1–5.
[15] K. A. Nagamatsu *et al.*, "Titanium dioxide/silicon hole-blocking selective contact to enable double-heterojunction crystalline silicon-based solar cell," *Appl. Phys. Lett.*, vol. 106, no. 12, 2015, Art. no. 123906.
[16] R. Islam, K. N. Nazif, and K. C. Saraswat, "Si heterojunction solar cells: A simulation study of the design issues," *IEEE Trans. Electron Devices*, vol. 63, no. 12, pp. 4788–4795, Dec. 2016.
[17] Y. Ing-Song, I. H. Chang, C. Hsyi-En, and L. Yung-Sheng, "Surface passivation of c-Si by atomic layer deposition TiO_2 thin films deposited at low temperature," in *Proc. IEEE 40th Photovolt. Specialist Conf.*, 2014, pp. 1271–1274.
[18] J. Jhaveri, S. Avasthi, K. Nagamatsu, and J. C. Sturm, "Stable low-recombination n-Si/TiO_2 hole-blocking interface and its effect on silicon heterojunction photovoltaics," in *Proc. IEEE 40th Photovolt. Specialist Conf.*, 2014, pp. 1525–1528.
[19] B. S. Richards, "Single-material TiO_2 double-layer antireflection coatings," *Solar Energy Mater. Solar Cells*, vol. 79, no. 3, pp. 369–390, 2003.
[20] A. Agrawal *et al.*, "Fermi level depinning and contact resistivity reduction using a reduced titania interlayer in n-silicon metal-insulator-semiconductor ohmic contacts," *Appl. Phys. Lett.*, vol. 104, no. 11, 2014, Art. no. 112101.
[21] J. Jhaveri *et al.*, "Hole-blocking crystalline-silicon/titanium-oxide heterojunction with very low interface recombination velocity," in *Proc. IEEE 39th Photovolt. Specialists Conf.*, 2013, pp. 3292–3296.
[22] R. Nicula, M. Stir, C. Schick, and E. Burkel, "High-temperature high-pressure crystallization and sintering behavior of brookite-free nanostructured titanium dioxide: In situ experiments using synchrotron radiation," *Thermochimica Acta*, vol. 403, no. 1, pp. 129–136, 2003.
[23] F. Yu, G. S. Han, Y. J. Tu, H. S. Roh, and J. K. Lee, "Electron extraction mechanism in low hysteresis perovskite solar cells using single crystal TiO_2 nanorods," *Solar Energy*, vol. 167, pp. 251–257, 2018.
[24] G. S. Han *et al.*, "Reduced graphene oxide/mesoporous TiO_2 nanocomposite based perovskite solar cells," *ACS Appl. Mater. Interfaces*, vol. 7, no. 42, pp. 23521–23526, 2015.
[25] E. J. Juarez-Perez *et al.*, "Role of the selective contacts in the performance of lead halide perovskite solar cells," *J. Phys. Chem. Lett.*, vol. 5, no. 4, pp. 680–685, 2014.
[26] C. Waldauf *et al.*, "Highly efficient inverted organic photovoltaics using solution based titanium oxide as electron selective contact," *Appl. Phys. Lett.*, vol. 89, no. 23, 2006, Art. no. 233517.
[27] S. Smit, D. Garcia-Alonso, S. Bordihn, M. S. Hanssen, and W. M. M. Kessels, "Metal-oxide-based hole-selective tunneling contacts for crystalline silicon solar cells," *Sol. Energy Mater. Sol. Cells*, vol. 120, no. Part A, pp. 376–382, 2014.